Journal of Chromatography, 550 (1991) 721–739
Elsevier Science Publishers B.V., Amsterdam

CHROMSYMP. 2295

Hydrodynamic and size-exclusion chromatography of polymers on porous particles

G. STEGEMAN, J. C. KRAAK and H. POPPE*
Laboratory for Analytical Chemistry, University of Amsterdam, Nieuwe Achtergracht 166, 1018 WV Amsterdam (Netherlands)

ABSTRACT

When packed columns filled with porous particles are used for the separation of macromolecules, either size-exclusion chromatography (SEC), hydrodynamic chromatography (HDC) or a combination of the two determine the migration rate. A simple theoretical model, assuming a stagnant pore liquid, was developed to describe a molecular weight calibration graph, which includes both HDC and SEC. In the overall calibration graph, there is a transition from the HDC calibration region at higher molecular weights to an SEC region at lower molecular weights. The smoothness of the transition depends on the ratio of the particle diameter to the pore diameter.

INTRODUCTION

The current interest in high-resolution separation methods for macromolecules and colloidal particles has brought about a number of important new developments. Promising new separation techniques such as field flow fractionation (FFF) [1] and capillary zone electrophoresis (CZE) [2] have shown potential in the development stage and are now being introduced in analytical laboratories. The more mature separation technique size-exclusion chromatography (SEC) has been made applicable to ultra-high-molecular-weight polymers by the development of particles with very large pore sizes. Hydrodynamic chromatography (HDC) on non-porous particles has developed into an inexpensive, high-speed fractionation technique for the sub-micrometre range, applicable to synthetic polymers, colloidal particles and large molecules of biological origin [3]. Of the four separation techniques mentioned, HDC has received least attention up to now. However, recently there has been renewed interest in HDC owing to the availability of 1–3-μm non-porous particles [4,5].

In HDC macromolecules are separated on the basis of their size owing to the hydrodynamic effect [6–10]. This effect occurs in a non-uniform flow profile such as is present in the inter-particle space in packed columns or in open capillaries. The centre of mass of large molecules is excluded from the low-velocity flow regions near the wall. As a result, large molecules migrate with a higher mean velocity than smaller molecules that can approach the wall more closely. Whether this hydrodynamic effect will lead to significant differences in migration rate depends on the aspect ratio, λ, which is the

0021-9673/91/$03.50

ratio of the solute radius to the radius of the flow channels. When λ is very small, the selectivity for polymer separation is low. Typically for $\lambda = 0.005$ the velocity increase is only 1% compared with infinitely small molecules [10]. On the other hand, when λ exceeds a maximum value (in practice about 0.35 for random coil polymers in packed columns), polymer recovery decreases and solutes may eventually block the column. The available volume for separation is accordingly limited, in practice between *ca.* $0.75V_0$ and V_0 [3,5,10], where V_0 is the total mobile phase volume.

In order to obtain suitable values for λ, the diameter of the flow channels should be adapted to the effective diameter of the solutes that are to be separated. For packed columns this means that the particle diameter determines the molecular weight working range. Recently, the use of 1.4–2.7-μm non-porous particles allowed the separation of polymers in the molecular weight range 10^4–10^7 [5]. In principle, particle diameters can be reduced still further to the submicrometre range, but column preparation and pressure drop might then pose problems. For practical reasons it therefore seems unlikely that HDC can be applied to molecular weights below 10^4 in the near future.

SEC has many features in common with HDC, such as the elution order and the limited elution volume range. However, the solute size range in SEC traditionally comprises smaller macromolecules than in HDC. SEC has been most succesful for polymers up to molecular weights of 10^6. Recent developments in SEC have been directed towards raising the upper molecular weight limit through the development of very wide-pore particles.

As HDC and SEC are increasingly covering the same molecular weight range, a sound comparison of both techniques is desired. A comparison based on experimental results was carried out a decade ago by Yau and Kirkland [11]. From evaluation of performance parameters such as the dynamic range, the specific resolution, the discrimination factor and the peak capacity, it was concluded that HDC is inferior to SEC in most areas. Recent developments in HDC make a re-evaluation of these parameters desirable and show that a more theoretical approach, exploring the limits of both techniques, is needed.

In several studies it was shown that SEC for the higher molecular weight range can be optimized when small particles with relatively large pores are employed [12–14]. This means that the inter-particle channels become relatively small compared with the polymers in the SEC working range and HDC effects are already emerging. This combination of HDC and SEC will be treated in detail in this paper. A simple theoretical model for the migration in HDC–SEC will be compared with experimental results. Advantages, prospects and limitations of combined HDC–SEC are also discussed.

THEORY

Polymer migration in SEC

In SEC, a general equation is valid for the retention volume, V_r, of eluted polymers:

$$V_r = V_0 + K_{SEC}V_i \tag{1}$$

where V_0 is the volume of the inter-particle (mobile) solvent, K_{SEC} is the SEC exclusion coefficient and V_i is the (stagnant) intra-particle pore volume.

In order to find expressions for K_{SEC}, several theories have been developed, describing the migration rate of polymers in SEC. Nowadays general agreement exists that size separations in SEC can be fully explained on a steric basis. This reduces the problem of SEC modelling to that of finding the best description of the intra-particle pore structure. The most versatile theoretical models in that respect are developed by Van Kreveld and Van den Hoed [15] and Knox and Scott [16]. They represent the porous packing particles by a structure built up from randomly placed uniform spheres and random-sized touching spheres, respectively. The model of Van Kreveld and Van den Hoed can be compared with experimental results more easily and is therefore applied in this paper.

In the randomly placed uniform spheres model (RSM), the radius of the elementary solid spheres, R_s, is related to the pore fraction of the porous system ψ and the total surface area per unit volume of porous material, S, according to

$$R_s = -\frac{3\psi}{S}\ln\psi \tag{2}$$

The particle porosity (or pore fraction) ψ is defined as

$$\psi = \frac{V_i}{V_i + V_s} \tag{3}$$

where V_s is the volume of the support material. ψ may in practice easily be obtained from the pore volume per weight unit of dry packing material and the skeleton density.

For a polymer with an effective radius r_i the accessible pore fraction ψ' will be

$$\psi' = \psi\left(\frac{R_s + r_i}{R_s}\right)^3 \tag{4}$$

The SEC exclusion coefficient is subsequently obtained from

$$K_{SEC} = \frac{\psi'}{\psi} \tag{5}$$

For a linear random coil polymer in a good solvent the effective polymer radius, r_i, can be calculated from the radius of gyration, r_g. For polystyrenes in tetrahydrofuran (THF), used in this work, the relationship between r_g and the weight-average molecular weight, M_w, is known. For r_i we can write [15]

$$r_i = \tfrac{1}{2}\sqrt{\pi}r_g = 1.23 \cdot 10^{-5} M_w^{0.588}\ (\mu m) \tag{6}$$

Polymer migration in HDC

In HDC on non-porous particles, the migration rate can be expressed by a relative quantity τ_{HDC}:

$$\tau_{HDC} = \frac{v}{v_p} = \frac{V_r}{V_0} \tag{7}$$

where v and v_p are the solvent and polymer migration velocity, respectively. The value of v can be calculated from the breakthrough time of a non-interacting low-molecular-weight molecule (marker) and the column length. For non-porous particles, v is equal to the interstitial velocity v_0.

For the transport of a dilute solution of finite-sized polymers in a cylindrical tube, it is assumed that polymer–wall interactions are absent and that the Poiseuille flow profile is essentially unaffected by the presence of the polymers. For rigid macromolecules, able to sample the accessible radial positions several times during their residence in the tube, τ_{HDC} is related to the aspect ratio, λ, according to [17]

$$\tau_{HDC} = (1 + 2\lambda - C\lambda^2)^{-1} \tag{8}$$

where λ is the ratio of the effective polymer radius r_i to the tube radius. The parameter C includes several hydrodynamic effects such as rotation of the polymer. In the different theoretical models C ranges between 1 and 5.3 [17], depending on the assumptions made in the model and on the type of solute.

Eqn. 8, originally derived for capillary HDC, was also able to predict the migration rate in packed columns when the inter-particle flow channels were represented as a parallel bank of equi-sized capillaries. The equivalent capillary radius was calculated in terms of the hydraulic radius of the packed bed, R_0, and consequently $\lambda = r_i/R_0$ [4,5]. For monodisperse spherical particles R_0 can be calculated from the particle diameter, d_p, and the (inter-particle) bed porosity, ε [3]:

$$R_0 = \frac{d_p}{3} \cdot \frac{\varepsilon}{1 - \varepsilon} \tag{9}$$

where $\varepsilon = V_0/(V_0 + V_p)$, V_p being the volume occupied by particles. Although eqn. 9 has been used frequently in the literature on HDC, monodispersity of the chromatographic beads cannot be assumed in many instances. When a column is filled with different sized spherical particles, R_0 can be calculated from a more general expression:

$$R_0 = 2 \cdot \frac{V_0}{A_0} = 2 \cdot \frac{V_p}{A_0} \cdot \frac{\varepsilon}{1 - \varepsilon} = \frac{\bar{d}_p}{3} \cdot \frac{\varepsilon}{1 - \varepsilon} \tag{10}$$

where A_0 is the total wetted surface area of the non-porous particles and $\bar{d}_p$ is the mean effective particle diameter; $\bar{d}_p$ is defined as [18]

$$\bar{d}_p = \frac{\int_0^\infty d_p^3 f(d_p) \mathrm{d}(d_p)}{\int_0^\infty d_p^2 f(d_p) \mathrm{d}(d_p)} \tag{11}$$

where $f(d_p)d(d_p)$ is the number fraction of particles having radii in the range d_p to $d_p + d(d_p)$. Eqn. 11 can be evaluated numerically using data from an experimentally obtained particle size distribution.

Polymer migration in HDC–SEC

When pore diameters of the SEC support particles are relatively large compared with the particle diameter, HDC effects may become of importance for the largest polymers in the SEC calibration range. Additional exclusion from low-velocity streamlines in the inter-particle space is then superimposed on pore exclusion. In a combined HDC–SEC curve, the smallest molecules are separated on basis of an SEC mechanism, whereas the largest molecules show differing migration rates due to HDC effects. In the intermediate size range both SEC and HDC determine the migration rate

A fundamental description of simultaneous SEC and HDC may lead to complex expressions for the migration rate. We present here a simple treatment by assuming that the flow profile and polymer hydrodynamics are essentially the same for flow in a bed of non-porous and porous particles. A necessary condition for this approximation is the absence of significant flow inside the particles. The effect of pores on polymer migration will only be viewed on a steric basis.

In line with the formalism used in HDC on non-porous particles, we again want to express the migration rate by the ratio of the solvent migration velocity to the polymer migration velocity τ. An expression for τ should be more general than eqn. 8 by also including SEC.

For porous particles, solvent and polymer molecules are distributed over the accessible parts of the mobile liquid in the inter-particle space and the stagnant liquid in the pores with a distribution coefficient of unity. The solvent and polymer migration velocities are thus averaged over the mobile and stagnant liquid fractions of the column, available to the solvent and the polymer molecules, respectively. The solvent migration velocity can therefore be represented as

$$v = v_0 \cdot \frac{V_0}{V_0 + V_i} \tag{12}$$

An expression for the polymer migration velocity is more difficult because the column volume accessible to the centre of mass of a polymer is restricted by both pore exclusion and exclusion from the wall in the inter-particle flow channels. As a first approximation we assume that exclusion from the wall in the inter-particle flow channels occurs as if no pores were present (Fig. 1). This means that the centre of mass of polymers is either in the pores or in the mobile liquid at a distance r_i from the wall. In fact we introduce an imaginary exclusion layer of thickness r_i in front of every pore entrace. This forbidden zone has no physical meaning, but it enables us to represent the migration rate in the inter-particle mobile liquid by expressions developed for HDC on non-porous beads. According to eqn. 7, the mean interparticle polymer velocity is thus equal to v_0/τ_{HDC}. From this inter-particle velocity, the accessible inter-particle volume and the accessible pore volume, we can calculate the polymer migration velocity:

$$v_p = \frac{v_0}{\tau_{HDC}} \cdot \frac{K_{HDC} V_0}{K_{HDC} V_0 + K_{SEC} V_i} \tag{13}$$

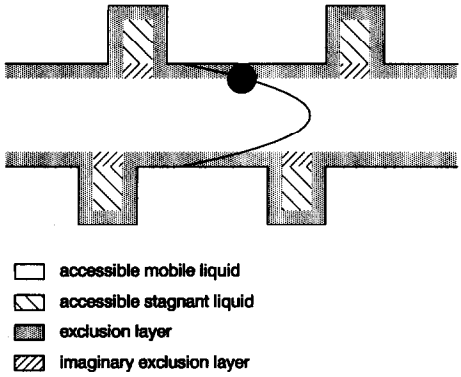

Fig. 1. Graphical clarification of the simple migration model for HDC–SEC.

where K_{HDC} is the fraction of the inter-particle volume that is accessible to the centre of mass of a polymer molecule. In the capillary model of the interstitial channels in a packed bed, we can write

$$K_{HDC} = \left(\frac{R_0 - r_i}{R_0}\right)^2 = (1 - \lambda)^2 \tag{14}$$

An expression for τ is found by combining eqns. 12, 13 and 14:

$$\tau = \tau_{HDC} \cdot \frac{V_0}{V_0 + V_i} + \tau_{HDC} \cdot \frac{K_{SEC} V_i}{(V_0 + V_i)(1 - \lambda)^2} \tag{15}$$

From this general expression for combined HDC–SEC, limiting forms are easily derived. For $\lambda = 0$ we arrive at an equation for pure SEC behaviour. For $V_i = 0$, HDC on non-porous particles is described. For $K_{SEC} = 0$, the migration behaviour is obtained for polymers being excluded from the pores.

Francis and McHugh [19] used a different approach to describe the migration rate in HDC–SEC by including force field effects and pore flow. In the limiting form for zero solute–wall interactions and zero pore flow, their general expression reduces to eqn. 15 except for the absence of the factor $(1 - \lambda)^2$. In practice, their expression will not give significantly different data, because the omitted factor is close to unity.

Refined migration model for HDC–SEC

The present migration model for HDC–SEC can be refined by permitting the presence of polymers between the pore entrance and $(R_0 - r_i)$ as shown in Fig. 2. Conserving simplicity, these partially pore-penetrated polymers are regarded as being in a stagnant liquid. Note that the velocity profile in the interstitial tube is still considered to be unchanged, leaving the migration of point molecules unaffected.

An expression for the volume of stagnant, partially penetrated polymers, $V_{0,s}$ is derived as follows. Rearrangement of eqn. 10 yields an expression for the outside surface area of the packing particles, A_0. A fraction of this surface constitutes pore

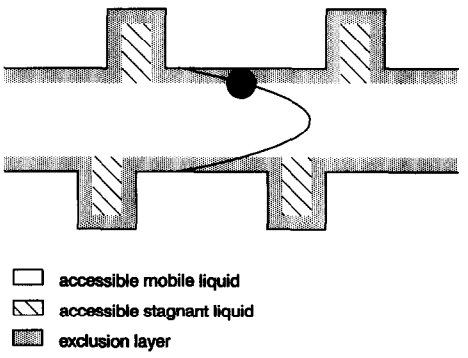

Fig. 2. Graphical clarification of the refined migration model for HDC–SEC.

entrances. We assume that this fraction is equal to ψ. Steric exclusion causes the cross-sectional pore area to be only partly accessible to the mass centre of polymers, the available part being approximately K_{SEC}. For $V_{0,s}$ we subsequently find

$$V_{0,s} = K_{SEC}\psi r_i A_0 = 2K_{SEC}\psi\lambda V_0 \tag{16}$$

The available volume in which polymers are stationary is the sum of $V_{0,s}$ and $K_{SEC}V_i$. An expression for τ can now be derived along the lines of the preceding migration model, yielding

$$\tau = \tau_{HDC} \cdot \frac{V_0}{V_0 + V_i} + \tau_{HDC} \cdot \frac{K_{SEC}(V_i + 2\psi\lambda V_0)}{(V_0 + V_i)(1 - \lambda)^2} \tag{17}$$

From eqn. 17, it is evident that the contribution from $V_{0,s}$ only becomes of importance

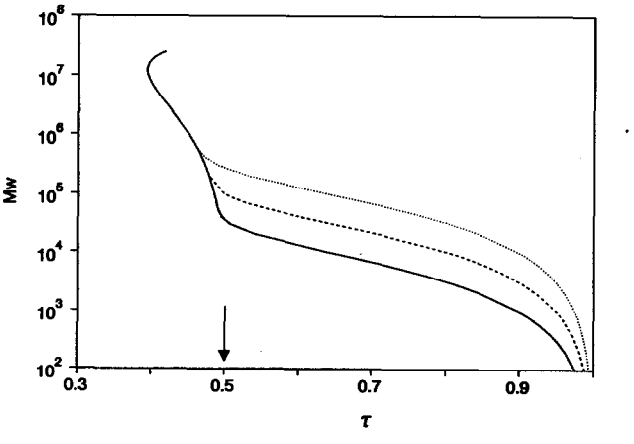

Fig. 3. Theoretical HDC–SEC calibration graphs for different pore radii. Curves are drawn for PS in THF according to eqn. 15. $d_p = 3\ \mu m$; $\varepsilon = 0.4$; $\psi = \frac{2}{3}$; R_p = (dotted line) 20 nm, (dashed line) 10 nm and (solid line) 5 nm. Arrow indicates τ value corresponding to the inter-particle space; $\tau = V_0/(V_0 + V_i)$.

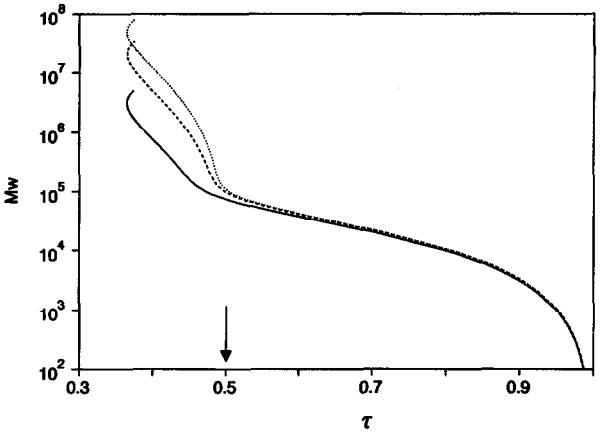

Fig. 4. Theoretical HDC–SEC calibration graphs for different particle diameters. R_p = 10 nm; d_p = (dotted line) 5 μm, (dashed line) 3 μm and (solid line) 1 μm. Other details as in Fig. 3.

for polymer sizes that are relatively large compared with the interstitial channels. In practice, $V_{0,s}$ may often be neglected, reducing eqn. 17 to eqn. 15.

Eqn. 15 was used to construct theoretical HDC–SEC calibration graphs in Figs. 3 and 4. The curves are drawn for polystyrenes in THF using eqn. 6 for the polymer radius. K_{SEC} was obtained employing the RSM model. For the polymer–solvent combination at hand, eqn. 8 for $C = 2.7$ gave good agreement with experimentally measured τ values on non-porous packing particles [5]. The assumptions made above on polymer hydrodynamics justify the use of this C value for polymer migration on porous particles also.

In Fig. 3, the effect of the pore radius on the calibration graph is shown for a constant d_p of 3 μm. For the smallest pore radius reflected, there is a clear distinction between the HDC and SEC calibration regions, although slight mutual overlapping is already present. On increasing the ratio of the pore radius to the particle diameter, R_p/d_p (*i.e.*, increasing the pore radius), the SEC and HDC region increasingly coincide. For the largest pore radius, it can be seen that HDC has a significant effect on the migration rate in the entire SEC molecular weight range.

The effect of the particle diameter for a fixed pore radius of 10 nm is represented in Fig. 4. Again, for the highest ratio R_p/d_p, the combined calibration graph shows the smoothest transition from the HDC region to a region dominated by SEC. For the 5-μm particles, the SEC and HDC regions appear fairly well separated. Calculations nevertheless show that HDC still has a notable influence on polymer migration near the exclusion limit. In order to eliminate these HDC effects, the R_p/d_p ratio should be further reduced. Only when this ratio is infinitely small is polymer separation due purely to a SEC mechanism. In that event, well known theoretical SEC calibration graphs appear, predicting coelution of all excluded polymers.

If eqn. 17 had been used instead of eqn. 15, the lower part of the calibration graph would have been shifted towards higher τ values. The largest shift in τ would have occurred for $\tau \approx 0.75$. However, this shift does not exceed an absolute value of 0.009 (or 1.2% relative), not even for the highest ratio R_p/d_p chosen. The use of eqn. 17 would therefore not have led to visibly distinct graphs.

Currently available SEC packing particles frequently reach R_p/d_p ratios such as those shown in Figs. 3 and 4. This means that nowadays many SEC calibration graphs are significantly affected by HDC effects. Indeed, in the literature chromatograms have appeared showing evident HDC effects [20,21], but these effects are mostly unnoticed or not understood. Such misinterpretations may lead to serious errors. Considerable errors may emerge when the SEC calibration graph is plotted as K_{SEC} *versus* log M_w. In that case V_0 needs to be determined, which is done by recording the elution volume of entirely excluded polymers. For these polymers, HDC effects are largest and the errors in V_0 (and in K_{SEC}) may be several percent [22]. In order to keep this HDC-induced error in V_0 within 1%, λ for an excluded polymer should not exceed 0.005 for $\varepsilon = 0.4$. For many popular SEC packing materials this condition cannot be fulfilled because the limiting λ value is already exceeded by polymers in the SEC dynamic range.

EXPERIMENTAL

Chemicals

Analytical-reagent grade THF and ethanol were obtained from Merck (Darmstadt, Germany). Prior to use these solvents were filtered through a 0.5-μm filter (Type FH; Millipore, Bedford, MA, USA).

Polystyrene standards (PS) with relative weight-average molecular weights, M_w, of (0.5–2750) · 10^3 and polydispersities as indicated by the supplier, ranging from 1.04 to 1.18, were obtained from Merck. Polystyrenes with M_w from 300 · 10^3 to 20 150 · 10^3 and polydispersities from 1.03 to 1.30 were purchased from Macherey, Nagel & Co. (Düren, Germany). Two polystyrene fractions with polydispersities of 1.01 and M_w of 43.9 · 10^3 and 775 · 10^3 were obtained from Toyo Soda (Tokyo, Japan). Polystyrene sample solutions of 0.005–0.02% (w/w) were prepared in THF.

Equipment

Chromatographic experiments were carried out using conventional high-performance liquid chromatography equipment. Solvent was delivered by a high-pressure liquid pump (Spectroflow 400; ABI, Ramsey, NJ, USA). A pneumatically driven injection valve with a 0.5-μl internal sample loop (Model Ci4W; VICI, Houston, TX, USA) was modified for high-speed switching by means of an HSSA kit (VICI). A variable-wavelength UV detector (Spectroflow 757; ABI) was adapted for detection on fused-silica capillaries according to Tijssen *et al.* [23]. A 100 μm I.D. capillary, which was directly coupled to the column outlet, served as a low-volume detection cell. The capillary length between the column and the detection cell was *ca.* 10 cm. An integrator (Type 3390A; Hewlett-Packard, Avondale, PA, USA) and a potentiometric recorder (Kompensograph 3; Siemens, Karlsruhe, Germany) were used for signal registration.

Columns

Three columns of 316 stainless steel with dimensions 150 × 4.6 mm I.D. (Chrompack, Middelburg, Netherlands) were packed with 3-μm porous silica particles (Hypersil; Shandon Scientific, Astmoor, Runcorn, UK) following a previously described packing procedure [5]. Two stainless-steel columns, 300 × 7.5 mm I.D.,

TABLE I

HYPERSIL DATA

$\bar{d}_p$ (μm)[a]	$\bar{R}_p$ (nm)	A_{spec} (m^2/g)	$V_{i,spec}$ (ml/g)	ρ_s (g/ml)	ψ	R_s (nm)[b]
3.39	6.0	143	0.634[c] 0.605[d]	2.19	0.582[c] 0.570[d]	7.22[c] 7.15[d]

[a] According to eqn. 11.
[b] According to eqn. 2.
[c] Data of the specific pore volume is determined for $R_p \leqslant 33$ nm.
[d] Data of the specific pore volume is determined for $R_p \leqslant 17$ nm.

containing experimental 3-μm polymeric PLRP-S particles (cross-linked polystyrene–divinylbenzene) with 100 and 300 Å pores, respectively, were a kind gift from Polymer Laboratories (Church Stretton, Shropshire, UK).

In order to verify the theoretical model for HDC–SEC migration, data on the columns and the packing materials were required. The measurements needed were only performed for the silica material, as the polymeric material is not sufficiently rigid. Data on the Hypersil packing material and on one column are listed in Tables I and II.

In Table I the mean effective particle diameter, $\bar{d}_p$, was calculated using a particle size distribution, determined by means of light diffraction (Mastersizer 20; Malvern, Malvern, UK). The mean pore radius, $\bar{R}_p$, and the pore-size distribution were obtained from mercury intrusion (Porosimeter 4000; Carlo Erba, Milan, Italy). The specific surface area, A_{spec}, according to the BET method and the specific pore volume, $V_{i,spec}$, of the packing material were determined by means of nitrogen adsorption (Sorptomatic 1800; Carlo Erba). The skeleton density of the silica support, ρ_s, was determined using a multi-volume helium picnometer (Model 1305; Micromeritics, Norcross, GA, USA). The particle porosity, ψ, was calculated from the specific pore volume and the skeleton density. R_s was calculated from the RSM, where S was obtained from A_{spec}, ρ_s and ψ.

In Table II the hold-up volume of the column ($V_0 + V_i$) was determined by weighing the column filled with ethanol and water. The density of ethanol was obtained using a density meter (Model DMA 10; Paar, Graz, Austria). The volume of the silica support, V_s, was calculated from the weighed column contents of Hypersil and the skeleton density. V_i was determined from the specific pore volume and the weight of the packing material. V_0 was calculated from the hold-up volume and V_i. As

TABLE II

DATA ON ONE COLUMN FILLED WITH HYPERSIL PARTICLES

$V_0 + V_i$ (ml)	V_s (ml)	V_i (ml)	V_0 (ml)	ε
1.808	0.640	0.890[a] 0.850[b]	0.918[a] 0.958[b]	0.374[a] 0.391[vb]

[a,b] As [c,d] in Table I.

a final check, the volume of the empty column was determined from the weighing experiment with ethanol and water. This value (2.456 ml) agreed very well with the sum of ($V_i + V_0$) and V_s from Table II (2.448 ml). The latter value was used for the calculation of ε.

The determination of the specific pore volume proved difficult as there is no clear distinction between the largest intra-particle pores and the smallest inter-particle pores. From the nitrogen adsorption isotherm and the pore-size distribution we concluded that the most appropriate value for the specific pore volume is determined when pores with radii up to 33 nm are included. For reasons to be explained later, we include in Tables I and II the specific pore volume for $R_p \leqslant 17$ nm and consequently the recalculated values for V_i, V_0, ψ, ε and R_s.

RESULTS AND DISCUSSION

HDC–SEC calibration graphs

In order to plot an experimental HDC–SEC calibration graph, τ was determined for a number of polystyrenes with various molecular weights. For this the ratio of the polymer elution time and the elution time for toluene was calculated. This ratio was multiplied by a correction factor to account for partial pore exclusion of the finite-sized toluene molecules. This correction factor is the τ value for toluene when we standardize on the column hold-up volume as determined by weighing. From accurate measurements of the elution volume of toluene and from the column hold-up volume (Table II), we calculated $\tau = 0.9475$ for toluene.

Previous work [5] showed that the magnitude of τ for high-molecular-weight PS depends on the flow-rate. With decreasing flow-rate, the peak maximum shifts to larger apparent molecular weights, until a constant τ value is reached. This flow-rate-dependent migration behaviour is not accounted for in the simple HDC models, but it is evident that these interferences only occur at higher velocities. In order to eliminate flow effects, we were therefore forced to work at low flow-rates. The

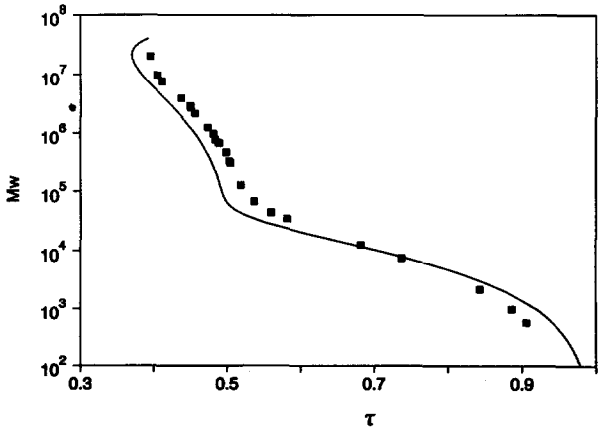

Fig. 5. Theoretical HDC–SEC calibration graph and experimental points for Hypersil packing particles. Details in the text and in Tables I and II ($V_{i,spec} = 0.634$ ml/g).

proper flow-rate settings were established by stepwise halving of the flow-rate until the decrease in τ was smaller than 0.001.

The theoretical calibration graph and the experimental points are presented in Fig. 5. The theoretical line was drawn according to eqn. 17, where K_{SEC} was calculated from the RSM model. From Tables I and II, we took the data that were calculated for a specific pore volume of 0.634 ml/g ($R_p \leqslant 33$ nm). From the graph it appears that the general shape of the experimental curve is predicted well by theory, although the fit is bad. For the entire HDC part, the theoretical line seems shifted to lower τ values compared with the experimental points. Such a parallel shift can, in our opinion, only be explained by a too large ratio V_i/V_0, caused by the uncertainty in the determination of the specific pore volume. We do not expect large errors in the determination of V_s and $V_0 + V_i$ (this is supported by the control measurement of $V_0 + V_i + V_s$).

When the specific pore volume is taken for pores up to 17 nm, we obtain a smaller V_i and consequently a smaller ratio V_i/V_0 (see Table II). The theoretical curve then shows a much better fit to the experimental points, as shown in Fig. 6. The agreement between theory and experimental points is fairly good, especially in the HDC part of the calibration graph. The experimental SEC curve shows a steeper gradient than the theoretical line. This is assumed to be a result of the pore-size distribution, which in the case of Hypersil cannot properly be accounted for by the RSM model. As was shown by Knox and Scott [16], the fit of the SEC part for Hypersil can be improved slightly when accounting for a range of pore sizes in the model. Such a modification makes the model complicated, whereas the improvement for the upper part of the SEC curve is only small.

As the validity of our simple HDC–SEC model hinges upon the fit of the curve near the SEC exclusion limit, Hypersil seems an unfortunate choice. A better fit of the SEC part can be expected for particles with a narrower pore-size distribution [16]. Moreover, for a narrow pore-size distribution, the migration model can be tested more accurately, because the specific pore volume is more reliably determined. Unfortunately, such particles are not easily available in a size range 1–3 μm.

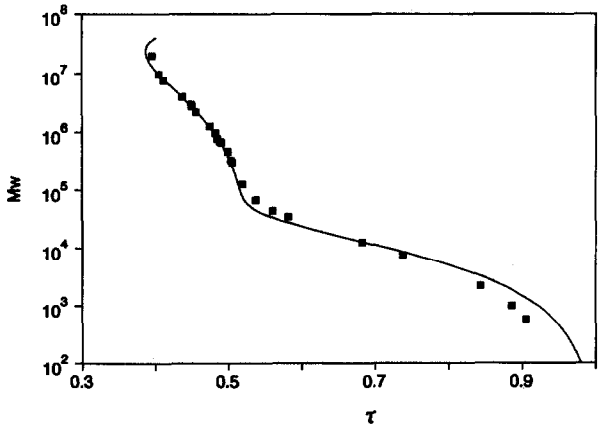

Fig. 6. Theoretical HDC–SEC calibration graph and experimental points for Hypersil packing particles. Details in the text and in Tables I and II ($V_{i,spec}$ = 0.605 ml/g).

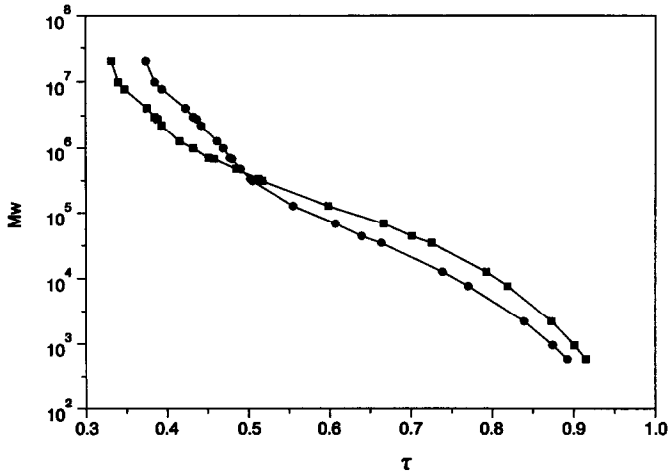

Fig. 7. Experimental HDC–SEC calibration graphs for polymeric packing particles (PL-RPS). $d_p = 3$ μm; R_p = (●) 5 nm and (■) 15 nm.

Unlike the rigid silica particles, porous polymeric beads cannot be fully characterized to test our migration model. Therefore, HDC–SEC on these materials is treated more qualitatively. As for silica particles, polymeric SEC particles smaller than 5 μm are not commercially available. However, the gift of two columns packed with experimental PS–DVB particles, having pore radii of 5 and 15 nm, respectively, enabled us to construct an experimental calibration graph for 3-μm particles. These graphs, shown in Fig. 7, are not corrected for pore exclusion of the marker (toluene). Again we observe that the combined curves cover a large dynamic molecular weight range. Compared with the silica material the SEC and HDC part are even more difficult to distinguish, as a result of the broad pore-size distribution. The intermingling of the HDC and SEC curves is most obvious for the packing with the widest pores. For equal V_i/V_0 and equal R_0, we would expect the HDC parts to coincide for the two columns. The parallel shift of the HDC parts can only be explained by an unequal ratio V_i/V_0. Apparently, for the material with 15-nm pores, the particle porosity was highest or these particles were more densely packed.

Column efficiency

A generalized plate-height equation for packed-column HDC can be written as

$$H = \frac{2\gamma D_m}{v_0} + \frac{2\beta_1 d_p}{1 + \beta_2 (v_0 d_p / D_m)^p} \tag{18}$$

where D_m is the molecular diffusion coefficient, γ, β_1 and β_2 are constants and the exponent p has distinct values in the various plate-height models: Giddings [24], $p = -1$; Huber [25], $p = -\frac{1}{2}$; Horváth and Lin [26], $p = -\frac{1}{3}$. At high linear velocities, dispersion is determined solely by convective mixing (*i.e.*, the second term in eqn. 18) and reaches a constant value of $2\beta_1 d_p$. At lower velocities, the contribution

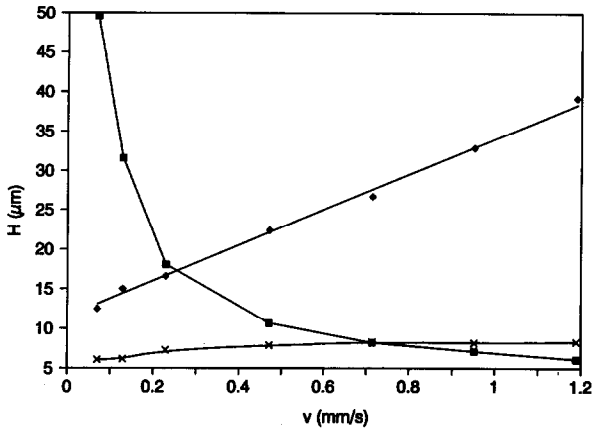

Fig. 8. Plate height *versus* solvent migration velocity on Hypersil packing particles. Solutes: (■) toluene, (◆) PS of M_w 43.9 · 10^3, (×) PS of M_w 775 · 10^3.

from longitudinal molecular diffusion (*i.e.*, the first term) may be significant, especially for fast-diffusing low-molecular-weight molecules.

In SEC, the plate-height equation contains an additional term accounting for resistance to mass transfer inside the particles [12,27]:

$$H = \frac{2\gamma D_m}{v_0} + \frac{2\beta_1 d_p}{1 + \beta_2 (v_0 d_p / D_m)^p} + \frac{V_0(V_r - V_0)d_p^2}{30 V_r^2 \gamma_s D_m} \cdot v_0 \qquad (19)$$

where γ_s is an obstructive factor for diffusion in the inner particle pores. For moderately high velocities the third term becomes the dominant plate–height term. In the high-velocity region where the analysis speed is greatest, plate heights in SEC thus far exceed those in HDC.

The different dispersion behaviours in HDC and SEC were verified experimentally for permeating and excluded solutes on a Hypersil column. The resulting curves of plate height *versus* solvent migration velocity are shown in Fig. 8. The solvent migration velocity instead of the inter-particle velocity was used because it could be calculated more accurately.

For toluene the plate height is mainly determined by longitudinal molecular diffusion, which is a result of the relatively high diffusion coefficient ($D_m = 2.66 \cdot 10^{-5}$ cm^2/s [28]). This causes H to decrease with increasing v whereas the minimum in the plate height curve is not yet reached at the highest solvent velocity in the graph. For PS of M_w 43.9 · 10^3, which is able to penetrate the intra-particle pores partly, longitudinal molecular diffusion is negligible ($D_m = 8.31 \cdot 10^{-7}$ cm^2/s [29]). The dominating plate-height contribution is the slow intra-particle mass transfer that causes H to increase in linear proportion to v. PS of M_w 775 · 10^3 ($D_m = 1.65 \cdot 10^{-7}$ cm^2/s [29]) is excluded from the pores. The plate height is exclusively determined by convective mixing and almost reaches a constant value at high velocities. In the investigated velocity range H is well below 9 μm.

The constant, low value for H in the HDC region shows that a large gain in

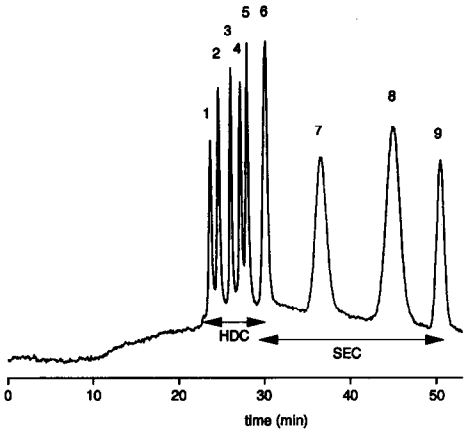

Fig. 9. HDC–SEC separation of polystyrenes on Hypersil particles. Column length = 45 cm (three columns coupled). Solutes: PS of M_w (1) $4000 \cdot 10^3$; (2) $2200 \cdot 10^3$, (3) $775 \cdot 10^3$; (4) $336 \cdot 10^3$; (5) $127 \cdot 10^3$; (6) $43.9 \cdot 10^3$; (7) $12.5 \cdot 10^3$; and (8) $2.2 \cdot 10^3$; and (9) toluene.

analysis time can be achieved at high v without sacrificing much efficiency. This provides important potential for high-speed separation of high-molecular-weight polymers. However, we shall meet an important proviso shortly, in terms of shear induced effects.

The dispersion and migration phenomena in HDC–SEC discussed so far are well illustrated by the separation of PS on Hypersil shown in Fig. 9. As can be seen, the combination of HDC and SEC yields a wide molecular weight dynamic range. In this instance the working range covers molecular weights from a few hundred to about $2 \cdot 10^7$, roughly the sum of the separate HDC and SEC ranges. When such a wide dynamic range is desired in SEC, a large pore-size distribution and consequently large particle diameters are required. However, the price that has to be paid for such an expanded dynamic range is a poorer column selectivity and larger plate heights, leading to poorer resolution. In combined HDC–SEC a large dynamic range is obtained while conserving high column selectivity and efficiency.

For the HDC–SEC columns in Fig. 9, a peak capacity of 66 was calculated [30] assuming a plate number of 75 000. From the chromatogram it appears that the number of fully resolved peaks is much lower. This can be explained by the polydispersity of the polymer samples, which largely determines the peak widths for most polymer fractions used [31]. In addition, for the calculation of the peak capacity we assumed a plate height of 6 μm for all polymer samples, which is certainly not true in the SEC region, as was shown by Fig. 8.

Effect of flow-rate

From the plate height–velocity curves in HDC–SEC, it appeared that high solvent migration velocities can be used without loss of column efficiency for the highest molecular weights. However, high flow-rates are often unfavourable for high-molecular-weight flexible polymers as shear degradation and deformation then become of importance.

In the literature on SEC, the subject of shear degradation has been treated frequently [32]. Although few experimental data on shear degradation have been published, it is well understood that one should be cautious not to use too high solvent velocities when analysing high-molecular-weight compounds. In HDC–SEC the avoidance of shear degradation restricts the solvent migration velocity even more than in SEC, because the molecular weights that can be determined are comparatively much higher.

Another effect of shear occurring at elevated flow-rates even before the limit of backbone breakage is reached is polymer deformation. When hydrodynamic forces are greater in magnitude than forces of chain relaxation arising from Brownian motion, the polymer chain is subjected to flow-induced stretching. The polymer diameter transverse to the direction of flow is then decreased, leading to higher τ values in HDC. Flow-rate-dependent data should be avoided whenever possible, so in HDC mobile phase velocities should be reduced to some critical value below which deformation is negligible.

Hoagland and Prud'homme [33,34] extensively studied shear-induced effects on polymer shape in HDC on non-porous particles. For partially hydrolysed polyacrylamide they found that the polymer size obtained from HDC decreased with flow-rate. Sample reinjection experiments at reduced flow-rates showed that degradation had not occurred. These results could be explained successfully by means of shear deformation using the Deborah number, *De*, the ratio of hydrodynamic forces to Brownian forces. They used the following expression for the Deborah number for flexible polymer chains in good solvents [33]:

$$De = k\left(\frac{\bar{v}}{d_p}\right)\frac{6.12\Phi\eta r_g^3}{RT} \tag{20}$$

where the constant k depends on the structure of the flow channels in the column, having an approximate nominal value $k = 6$ [35]. The superficial solvent velocity is $\bar{v}$, Φ is the Flory–Fox parameter (*ca.* $2.5 \cdot 10^{23}$ mol^{-1}), η is the solvent viscosity, r_g is the radius of gyration of the polymer at equilibrium, R is the gas constant and T is the temperature. At $De < 0.1$ molecular stretching can be considered insignificant and the polymer has its equilibrium diameter. At $De = 0.1$, there is an onset of deformation and at $De = 0.5$ a critical elongation rate is reached where coiled polymers are transformed into extended fibre-like chains [33].

For the experimental HDC–SEC calibration graph we were able to avoid flow-rate-dependent τ values by choosing sufficiently low flow velocities. For the Hypersil column some additional measurements of τ at higher flow-rates were carried out for PS of M_w $9800 \cdot 10^3$. According to eqn. 20, this polymer starts to deform at $\bar{v} = 0.033$ mm/s ($De = 0.1$), which corresponds to a solvent migration velocity $v = 0.044$ mm/s.

The results in Table III show an increase in τ with solvent velocity. This is in accordance with the coil-stretch theory and indicates shear deformation at higher velocities. At the highest flow-rate settings the chromatograms showed an apparent bimodal molecular weight distribution with two peak maxima. This is reflected in the table by two τ values in the last column. In order to check whether shear degradation had occurred, all eluted samples were collected and reinjected at the lowest flow-rate

TABLE III

EFFECT OF THE SOLVENT MIGRATION VELOCITY ON τ FOR PS OF M_w $9800 \cdot 10^3$

Column: Hypersil.

v (mm/s)	De^a	τ
0.031	0.089	0.427
0.059	0.13	0.427
0.073	0.16	0.435
0.14	0.32	0.451
0.29	0.65	0.464/0.499
0.58	1.3	0.481/0.602

[a] De = Deborah number according to eqn. 20.

setting. The τ values obtained were now equal to those for the original sample, demonstrating that shear degradation was not yet of importance in the selected flow-rate range. We cannot yet explain the double peaks at high velocities.

CONCLUSIONS

In the molecular weight calibration graph for porous packing particles with relatively wide pores there is a gradual transition from a region dominated by SEC to an HDC region. An experimentally obtained HDC–SEC calibration graph for porous silica particles was successfully described by a migration model where the inter-particle flow channels were represented as open tubes while the intra-particle structure was depicted by the random uniform spheres model. This model also showed that HDC already has a significant effect on polymer migration in many currently available SEC columns.

The advantages of combined HDC–SEC over separate operation are a higher peak capacity and an expanded molecular weight dynamic range.

In HDC (and in HDC–SEC) shear rates are sufficiently high to cause stress-induced changes in polymer conformation. This forms a serious restriction for the high-speed analysis of high-molecular-weight flexible polymers. Shear deformation of high-molecular-weight polystyrenes was demonstrated by an increase in τ with solvent velocity.

Further studies on HDC–SEC should be aimed at the development and testing of small monodisperse porous particles with a narrow pore-size distribution. The validity of the migration model remains to be tested for various d_p/R_p ratios. The assumed stagnancy of the pore liquid should be checked and possible effects of pore flow on migration and dispersion should be evaluated.

SYMBOLS

A_0 wetted surface area in a bed of non-porous particles

A_{spec} specific surface area

De	Deborah number
D_m	molecular diffusion coefficient
d_p	particle diameter
H	theoretical plate height
K_{HDC}	accessible fraction of the inter-particle space
K_{SEC}	accessible fraction of the intra-particle pores (SEC exclusion coefficient)
k	constant accounting for the structure of the flow channels in a packed column.
M_w	weight-average molecular weight
R	gas contant
R_0	hydraulic radius of the packed bed
R_p	pore radius
R_s	radius of an elementary solid sphere in the RSM
r_g	radius of gyration
r_i	effective polymer radius
S	surface area per unit volume of a porous system
T	absolute temperature
V_0	inter-particle solvent volume
$V_{0,s}$	volume containing stagnant partially penetrated polymers
V_i	intra-particle (pore) volume
$V_{i,spec}$	specific pore volume
V_p	volume occupied by particles ($= V_i + V_s$)
V_r	retention volume
V_s	volume of the solid support material
v	solvent migration velocity
$\bar{v}$	superficial solvent velocity
v_0	inter-particle solvent velocity
v_p	polymer migration velocity
$\beta_1,\beta_2,\gamma,\gamma_s$	constants in the plate-height equation
ε	bed porosity $= V_0/(V_0 + V_p)$
η	solvent viscosity
λ	aspect ratio, r_i/R_0
ρ_s	skeleton density of the solid support material
τ	relative migration rate in HDC–SEC
τ_{HDC}	relative migration rate in HDC
Φ	Flory–Fox parameter
ψ	pore fraction of porous particles (or particle porosity)
ψ'	pore fraction accessible to a finite-sized molecule

ACKNOWLEDGEMENTS

The authors thank Dr. F. P. Warner, Polymer Laboratories, for the kind gift of two packed columns. Mrs. Mittelmeijer-Hazeleger is thanked for characterizing the silica particles.

REFERENCES

1 W. G. Kuhr, *Anal. Chem.*, 62 (1990) 403R.
2 K. D. Caldwell, *Anal. Chem.*, 60 (1988) 959A.
3 A. J. McHugh, *CRC Crit. Rev. Anal. Chem.*, 15 (1984) 63.
4 J. C. Kraak, R. Oostervink, H. Poppe, U. Esser and K. K. Unger, *Chromatographia*, 27 (1989) 585.
5 G. Stegeman, R. Oostervink, J. C. Kraak, H. Poppe and K. K. Unger, *J. Chromatogr.*, 506 (1990) 547.
6 E. A. DiMarzio and C. M. Guttman, *J. Polym. Sci.*, 7 (1969) 267.
7 E. A. DiMarzio and C. M. Guttman, *Macromolecules*, 3 (1970) 131 and 681.
8 H. Small, *J. Colloid Interface Sci.*, 48 (1974) 147.
9 A. W. J. Brough, D. E. Hillmann and R. W. Perry, *J. Chromatogr.*, 208 (1981) 175.
10 D. C. Prieve and P. M. Hoysan, *J. Colloid Interface Sci.*, 64 (1978) 201.
11 W. W. Yau and J. J. Kirkland, *J. Chromatogr.*, 218 (1981) 217.
12 J. C. Giddings, *Adv. Chromatogr.*, 20 (1982) 217.
13 G. Guiochon and M. Martin, *J. Chromatogr.*, 326 (1985) 3.
14 H. Engelhardt and G. Ahr, *J. Chromatogr.*, 282 (1983) 385.
15 M. E. van Kreveld and N. van den Hoed, *J. Chromatogr.*, 83 (1973) 111.
16 J. H. Knox and H. P. Scott, *J. Chromatogr.*, 316 (1984) 333.
17 R. Tijssen, J. Bos and M. E. van Kreveld, *Anal. Chem.*, 58 (1986) 3036.
18 W. J. Beek and K. M. K. Muttzall, *Transport Phenomena*, Wiley, London, 1980, p. 119.
19 D. C. Francis and A. J. McHugh, *ACS Symp. Ser.*, No. 245 (1984) 3.
20 J. J. Kirkland, *J. Chromatogr.*, 125 (1976) 231.
21 J. H. Knox and F. McLennan, *J. Chromatogr.*, 185 (1979) 289.
22 G. Stegeman, J. C. Kraak and H. Poppe, in preparation.
23 R. Tijssen, J. P. A. Bleumer and M. E. van Kreveld, *J. Chromatogr.*, 260 (1983) 297.
24 J. C. Giddings, *J. Chromatogr.*, 5 (1961) 61.
25 J. F. K. Huber, *J. Chromatogr. Sci.*, 7 (1969) 85.
26 Cs. Horváth and H. Lin, *J. Chromatogr.*, 126 (1976) 401.
27 J. C. Giddings, L. M. Bowman, Jr., and M. N. Myers, *Macromolecules*, 10 (1977) 443.
28 R. C. Reid, J. M. Prausnitz and T. K. Sherwood, *The Properties of Gases and Liquids*, McGraw-Hill, New York, 3rd ed., 1977.
29 W. Mandema and H. Zeldenrust, *Polymer*, 18 (1977) 835.
30 E. Grushka, *Anal. Chem.*, 42 (1970) 1142.
31 J. H. Knox and F. McLennan, *Chromatographia*, 10 (1977) 75.
32 H. G. Barth and F. J. Carlin, Jr., *J. Liq. Chromatogr.*, 7 (1984) 1717.
33 D. A. Hoagland and R. K. Prud'homme, *Macromolecules*, 22 (1989) 775.
34 D. A. Hoagland and R. K. Prud'homme, *J. Appl. Polym. Sci.*, 36 (1988) 935.
35 W. M. Kulicke and R. Haas, *Ind. Eng. Chem., Fundam.*, 23 (1984) 308.